Applied Physics B (2023) 129:47
https://doi.org/10.1007/s00340-023-07989-x

Applied Physics B
Lasers and Optics

RESEARCH

Power-scaled CW Alexandrite lasers

Goronwy Tawy[1,2] · Ara Minassian[3] · Michael J. Damzen[1]

Received: 29 November 2022 / Accepted: 5 February 2023 / Published online: 1 March 2023

Abstract
We present several strategies for increasing the output laser power of near-diffraction limited continuous-wave Alexandrite lasers pumped by fibre-coupled red laser diodes. Laser mode size control using a convex mirror with the varying thermal lens is shown to be an efficient method for generating record levels of output power from a diode-pumped Alexandrite laser. 8.6 W is obtained with $M^2 < 1.1$ and an optical efficiency of 27%. 735–790 nm wavelength tuning is demonstrated with > 2.5 W and a record dual-wavelength output power of 4.2 W. In a ring-cavity geometry, 5.1 W is obtained with $M^2 < 1.1$ showing promising potential for multi-watt single-longitudinal-mode operation. Detailed laser cavity modelling including thermal lens analysis is also provided.

1 Introduction

Cr^{3+}:$BeAl_2O_4$, commonly known as Alexandrite, is a vibronic laser emitting at around 720–820 nm with excellent thermo-mechanical properties (e.g. $K_c = 23\,\mathrm{Wm^{-1}\,K^{-1}}$, $dn/dT = 6 \times 10^{-6}\,\mathrm{K^{-1}}$) [1]. As with other Cr^{3+}-doped gain media, the absorption of Alexandrite is characterised by two broad and strong peaks at the blue and red region of the visible spectrum. These properties make diode-pumped Alexandrite a highly promising efficient and compact laser operating in continuous-wave (CW) [2], Q-switched [3, 4] and mode-locked [5] regimes.

Diode-pumped Alexandrite lasers are mostly used in Q-switching applications due to its ability to directly generate mJ levels of pulse energy in the $700 - 800$ nm region, which cannot be obtained directly from other diode-pumped laser gain media [3].

In the CW regime, low to mid-power ($1\,\mathrm{mW} - 1\,\mathrm{W}$) and high brightness ($M^2 < 1.2$) applications are often well addressed by commercially available narrow linewidth diode lasers or Ti:Sapphire lasers with the latter also providing greater wavelength coverage. Ti:Sapphire lasers, however, are often expensive, bulky and not well suited to applications outside the laser laboratory due to its water cooling requirements. Though diode pumping is possible, the use of blue diodes has been shown to lead to parasitic issues and research on green-diode pumping is limited [6]. Other Cr-doped gain media such as Cr:LiSAF and Cr:LiCAF have reported $2 - 3$ W of CW laser power [7–9], though further power scaling is challenging due to its weaker thermo-mechanical properties.

Power scaling of diode-pumped solid-state lasers to > 5 W across the tuning band provides greater versatility for quantum technology applications such as Rb-cooling atom interferometry [10]. Additional applications such as single-step conversion to the UVA band and a high-brightness pump source for ultra-fast Tm-doped lasers, an area that has become a highly topical area of research [11, 12], are also of particular interest. These power levels are at the limit of commercial Ti:Sapphire lasers and frequency doubled EDFA systems have limited spectral coverage.

In our previous work, we demonstrated > 5 W TEM_{00} operation from a diode-pumped Alexandrite laser [2]. This paper builds and expands on that work with a more detailed analysis of the thermal lensing, cavity modelling as well as introducing new cavity geometries. Thermal lensing in Alexandrite is complex due to the presence of excited state absorption (ESA) which is both temperature and wavelength dependent [13]. Wavefront measurements of the lens dioptric power have also shown that the pump power dependence does not agree with the quantum defect and ESA effects,

✉ Goronwy Tawy
goronwy.tawy12@imperial.ac.uk

[1] Photonics Group, The Blackett Laboratory, Imperial College London, London SW7 2AZ, UK

[2] Optoelectronics Research Centre, University of Southampton, University Road, Southampton SO17 1BJ, UK

[3] Unilase Ltd., 60 Gray's Inn Road, Unit LG04, London WC1X 8LU, UK

but with another contribution present. We have attributed this additional contribution as being related to the refractive index distribution of the excited ions. Altogether, this makes pump-induced lensing in Alexandrite a significant factor in power scaling. Instead of minimising the thermal lens, this work looks at using it as a focusing element to simplify the cavity design for achieving record levels of CW power across the tuning range of Alexandrite.

2 Alexandrite linear laser cavity

2.1 Plane–Plane cavity

The most straightforward and compact cavity design is a plane–plane laser cavity with the thermal lens of the laser gain medium providing the mode size control. Figure 1 shows the setup for the plane–plane cavity. The gain medium is a 0.2 at.% Cr-doped Alexandrite crystal (Crystech) with dimensions of $4 \times 4 \times 6\,\text{mm}^3$. The crystal is mounted in a water-cooled copper heatsink. The cavity is formed of two dichroic mirrors (DM) which are highly transmissive (HT) at the pump wavelength (640 nm) and highly reflective (HR) at the laser wavelength ($720 - 820\,\text{nm}$), and an output coupler (OC) with reflectivity R_{OC}.

Pumping is provided by a fibre-coupled (200 µm) laser diode (LD) which emits at around 640nm (FWHM = 1.5 nm) with a maximum unpolarised output power of 40 W ($M^2 = 100$). Throughout this work, the fibre output is collimated with a 35nm collimator and focused to a waist w_p located at the crystal surface. The absorption coefficient is measured to be around $6\,\text{cm}^{-1}$ and 0.3cm^{-1} along the *b*-axis and *a*-axis, respectively. Around 70% of the pump is absorbed after a single pass. The transmitted pump is retro-reflected using a curved mirror (CM) and a quarter-wave plate which on double pass rotates the transmitted pump that was primarily along the crystal a-axis to the b-axis.

The output characteristics of the three-mirror laser were measured with $R_{OC} = 98\%$ and a crystal temperature of $T_A = 20°\text{C}$. Figure 2 shows the results with $L_1 = 5\,\text{mm}$, $L_2 = 10\,\text{mm}$ (measured from left crystal facet) and $w_p = 150\,\mu\text{m}$. 12.2 W was obtained at 34.9 W absorbed pump power with a slope efficiency of 38.3%. The laser mode quality was measured to be $M_x^2 = 5.7$ and $M_y^2 = 6.3$ at the maximum laser power, though it was near-diffraction limited at around 1–2 W of laser power.

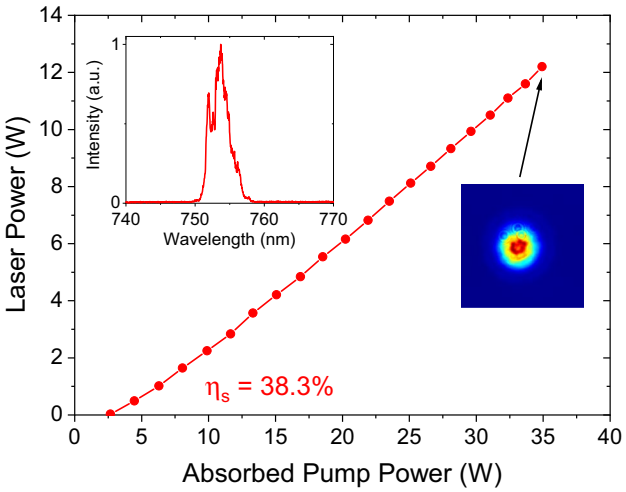

Fig. 2 Power curve for compact plane–plane cavity

Improved mode quality can be obtained with better matching of the pump and laser mode sizes. The laser mode size can be increased for better matching at higher power by increasing the cavity length. With $L_1 = 15\,\text{mm}$, $L_2 = 30\,\text{mm}$ and $w_p = 225\,\mu\text{m}$ (where the latter has been increased to minimise damage on the mirrors), 10 W was obtained at 34.9 W absorbed pump power with a slope efficiency of 35.5%. The laser mode quality was measured to be $M^2 < 2.6$ (in both directions) at the maximum laser power.

2.2 Convex-plane cavity

For further improvement in mode quality, a simple method to mitigate the strong thermal lens is to use a convex mirror. We recently demonstrated that using a convex-plane cavity can provide > 5 W with near-diffraction limited TEM_{00} output mode quality [2]. Here, we present further details of the cavity model, results and analysis.

Figure 3 shows a schematic of the laser cavity setup. The cavity is formed of convex DM mirror with curvature *R* and a plane OC. The mirror positions L_1 and L_2 play an important

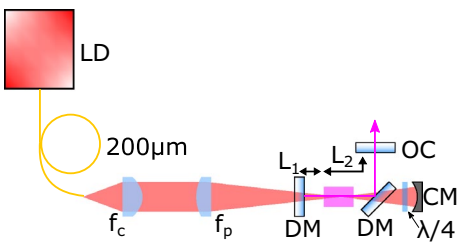

Fig. 1 Diode-pumped Alexandrite laser

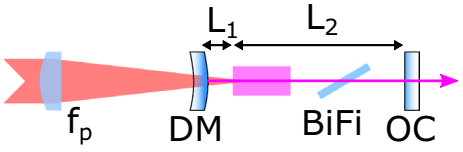

Fig. 3 Convex-plane Alexandrite laser cavity

role in determining the output mode profile with a preference to slightly underfill the pump mode size at the gain medium. An understanding of the thermal lens strength is, therefore, essential to obtaining highly efficient TEM_{00} operation.

The dioptric power of the thermal lens can be directly measured using a Shack-Hartmann wavefront sensor or approximated using an analytical model [13]. Figure 4 shows the measured dioptric power as a function of the absorbed pump power for the convex-plane cavity with $w_p = 150\,\mu m$ and $w_p = 300\,\mu m$ (for further details of the experiment, see [14]). Predictions of the dioptric power for other pump sizes can be made with the help of the analytical model in combination with these measurements.

Figure 5 shows the laser mode size as a function of the thermal lens with $L_1 = 5\,mm$ and $R = -300\,mm$. The cavity is stable at $f \approx 300\,mm$; however, laser threshold occurs when the thermal lens is slightly stronger due to mode matching. The model predicts threshold to be at a thermal lens focal length of $f \approx 200\,mm$ and increasing to $f \approx 100mm$ at around 18 W of absorbed pump power. For TEM_{00} operation, it is preferential to slightly under-fill the pump mode; therefore, $L_2 = 50\,mm$ was chosen to provide good matching to a pump size of $w_p = 225\,\mu m$ as well as good sensitivity to the change in thermal lens with increased pump power.

5.45 W was obtained at 17 W absorbed pump power with a near-diffraction limited mode quality of $M^2 < 1.1$, as shown in Fig. 6. The shape of the power curve can be attributed to the variation in the thermal lens. Figure 7 shows the measured dioptric power as a function of the absorbed pump power for the convex-plane cavity (green). This was calculated from the measured laser mode size at the OC.

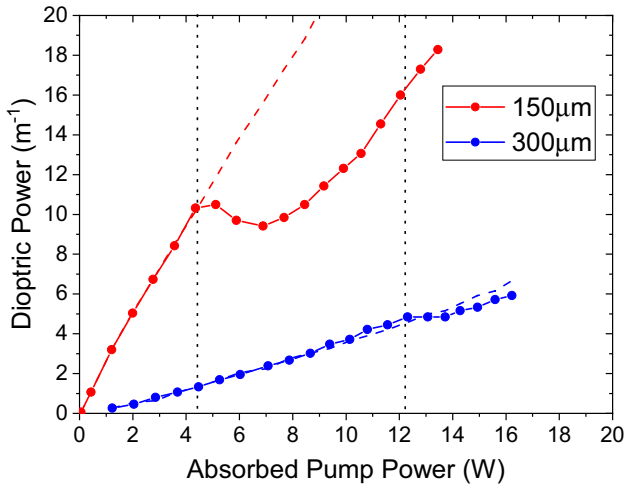

Fig. 4 Measured dioptric power as a function of absorbed pump power for $w_p = 150\,\mu m$ and $w_p = 300\,\mu m$ with dashed line showing non-lasing trend. Dotted black line indicates laser threshold

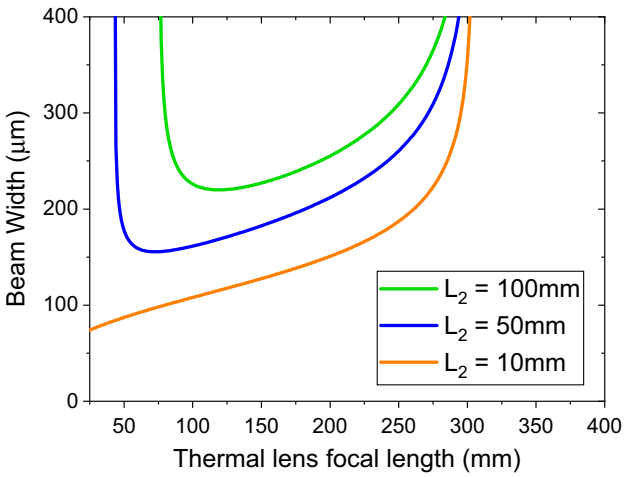

Fig. 5 Theoretical laser beam width radius at crystal as a function of thermal lens focal length for convex-plane cavity

The theoretical dioptric power under non-lasing conditions is also shown (dashed green line).

At $10 - 13\,W$, the dioptric power is relatively unchanged at around $5m^{-1}$ ($f = 200\,mm$), whereas under non-lasing conditions, the dioptric power would continue to increase. This deviation from that under non-lasing conditions is attributed to a combined contribution of a thermal lens and the lens due to the distribution of the excited ions (a population lens) [13].

Above threshold, the population is fixed due to the clamped inversion. It is possible that just above threshold, only the central distribution of the inversion is clamped with the outer region still increasing. This would contribute to a negative lensing effect and give rise to a levelling out or even reduction in the total measured dioptric power until further

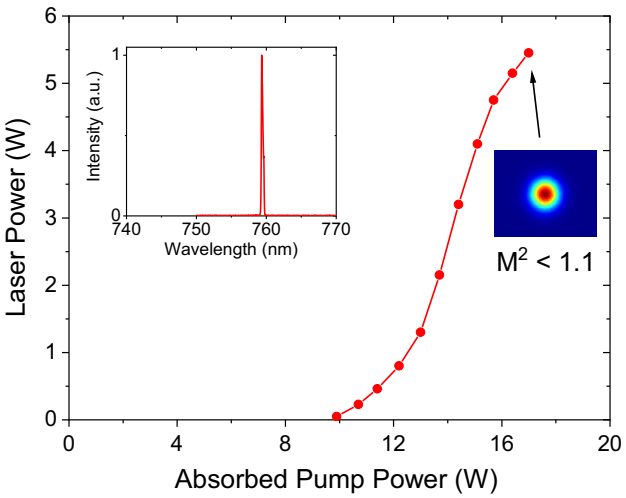

Fig. 6 Power curve for convex-plane cavity

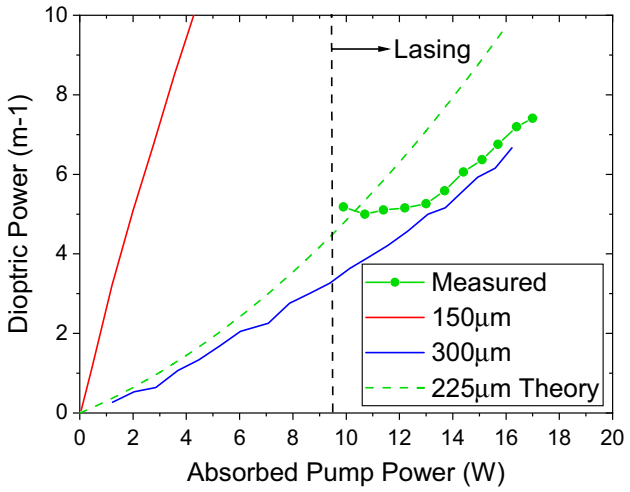

Fig. 7 Dioptric power as a function of absorbed pump power for $w_p = 225\,\mu m$ under lasing conditions (calculated from laser mode size at OC) and under non-lasing conditions (theoretical)

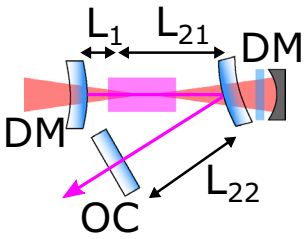

Fig. 8 Double convex-plane cavity

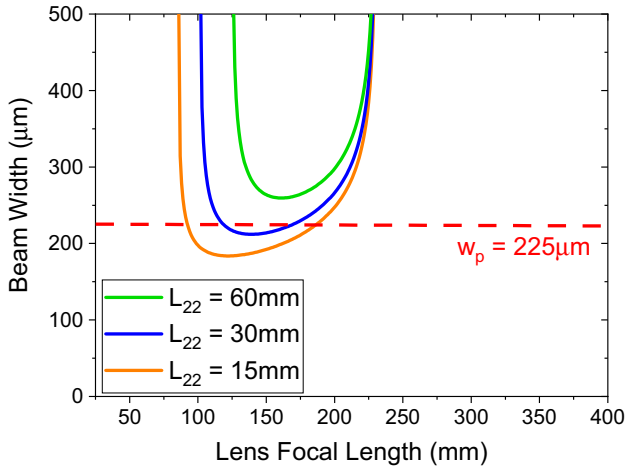

Fig. 9 Theoretical laser beam width radius at crystal as a function of thermal lens focal length for double convex-plane cavity

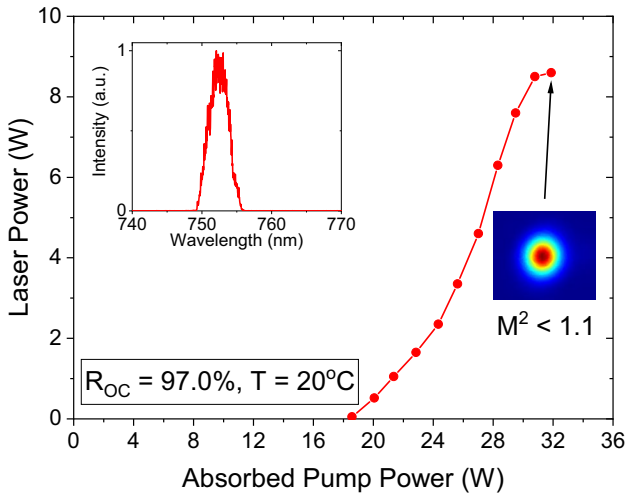

Fig. 10 Power curve for double convex-plane cavity

increase in the contribution of the thermal lens. This is also evident for $w_p = 150\,\mu m$ as shown in Fig. 4.

At $13 - 15\,W$ the dioptric power increases and provides better matching to the pump mode allowing better power extraction and a higher local slope efficiency. This enables high level of output power with the under-filling of the pump size enabling excellent mode operation, as shown in Fig. 6.

At higher pump power (or stronger thermal lens), the laser power begins to plateau before either roll-over or increasing in multi-mode operation. Increasing the pump waist size alleviates the thermal lens but increases the threshold pump power. A power-scaling approach would be to increase the pump waist size and convex mirror curvature; however, at the time of this work, only the $R = -300\,mm$ mirror was available.

An alternative strategy for increasing the laser power further was to incorporate a retro-reflection system with an additional convex mirror for mitigation of the thermal lens on both sides of the crystal, as shown in Fig. 8. The second convex mirror is tilted at a small angle ($\sim 10°$) to complete a three-mirror cavity. Due to the additional complexity of the system, the mode size of the laser cavity was modelled by numerically solving the ABCD Gaussian propagation formula at a reference plane after a single round trip.

Figure 9 shows the results of the model with $L_1 = 5\,mm$, $L_{21} = 35\,mm$ and $R = -300\,mm$ for both mirrors. $L_{22} = 15\,mm$ provides the largest stability range from around $f = 225\,mm$ to $f = 75\,mm$ as well as suitable under-filling of the $w_p = 225\,\mu m$ pump size.

Figure 10 shows the results for the three-mirror cavity with $L_{22} = 15\,mm$. A maximum laser power of 8.6 W at 31.9 W absorbed pump power was obtained corresponding to an optical efficiency of 27%. The output mode was again excellent with $M^2 < 1.1$ with a broad spectrum (FWHM = 4 nm) centred at 753 nm.

This system was limited by the available pump power, though the power did plateau at the maximum pump power.

Using the model, it is predicted that the dioptric power ranged from around 10 m^{-1} at threshold to 13 m^{-1} ($\approx$ 75 mm) at the maximum power, therefore approaching the edge of stability. With further optimisation in waist size and mirror curvature, it is believed that 10 W can be obtained. Optimisation of the crystal doping and length would also provide further improvement in power scaling performance such as by lowering the doping level (as found in [15]) though this has not been investigated in this work.

Wavelength tuning and dual-wavelength operation were investigated using an intra-cavity birefringent filter (BiFi), as shown in Fig. 3. Figure 11 shows the laser power as a function of wavelength using a 1 mm thick BiFi. A continuous tuning range of 735–790 nm was achieved (limited by the free spectral range) with a linewidth of < 0.5 nm and a beam quality of M^2 < 1.1 across the entire tuning range. The output power was > 2.5 W over the entire tuning range (17 W absorbed pump power)—superior to any other diode-pumped vibronic laser in the 700–800 nm region. Figure 12 shows the laser spectrum when operating at dual wavelength operation with a peak-to-peak separation of 57 nm and an output power of 2.75 W. 4.2 W of dual wavelength operation with a 15.5 nm separation was also obtained using a 4 mm thick BiFi.

The long-term power stability of these laser cavities (and those that will be presented later) was analysed by measuring the maximum laser power over a 1-h period with a power stability of < 1% relative standard deviation. Fluctuations in the wavelength in the tunable lasers were within the resolution of the spectrometer. No self-pulsing was observed in all systems when analysing the output on the microsecond scale.

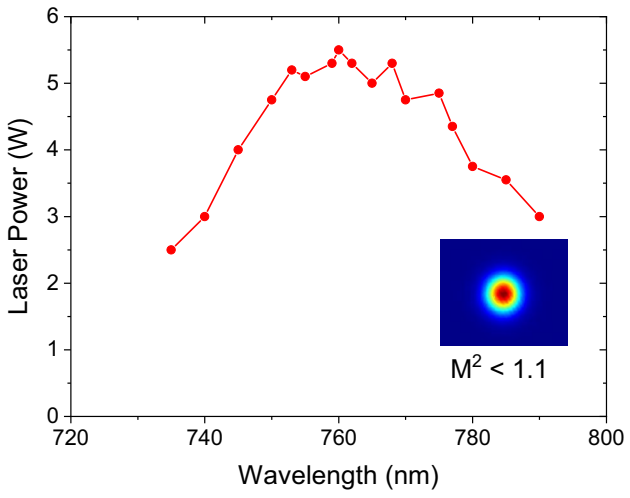

Fig. 11 Laser power as a function of wavelength using 1 mm thick BiFi

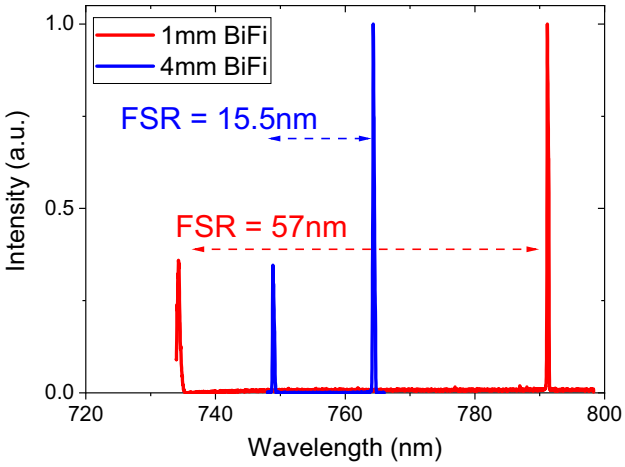

Fig. 12 Spectra at dual wavelength operation for 1 mm and 4 mm thick BiFis

3 Alexandrite ring laser cavity

For narrow-linewidth applications, single-longitudinal-mode (SLM) operation is necessary. The large emission bandwidth of Alexandrite makes SLM microchip lasers challenging, and methods such as the twisted mode technique work only for isotropic gain media. SLM operation is preferentially obtained using a unidirectional laser cavity in a ring configuration to eliminate spatial hole burning.

The ring geometry formed of two curved optics and two planar optics (often in a bow-tie geometry) is the most typical ring laser design. This configuration provides good mode matching between a near-diffraction limited pump and a tightly focused laser mode as well as good alignment stability. Our group has developed two systems that achieved > 1 W SLM with wavelength tuning using a low-brightness diode bar [16, 17]. However, further power scaling is challenging due to the relatively low efficiency of the system and the increasing aberration contribution from the poor intensity distribution of the diode bar.

Using a fibre-coupled pump source with an increased waist size to alleviate the thermal lensing does not easily match to the mode size dynamics of the bow-tie geometry. The aim, therefore, is to use a cavity geometry that allows good mode matching for larger pump sizes and as shown previously, to use the thermal lens for mode size control.

Figure 13 shows a schematic of the experimental setup. The cavity is formed of four plane mirrors: two DMs, a HR mirror and an OC. Two methods for mode size control are considered, first, with an intra-cavity negative (diverging) lens of focal length $f_{-} = -250$ mm, and then without the negative lens.

The mode size of the laser cavity can be modelled by numerically solving the ABCD Gaussian propagation

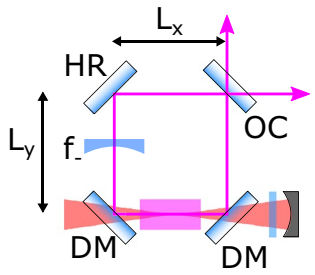

Fig. 13 Alexandrite ring laser setup with intra-cavity lens of focal length f_{-}

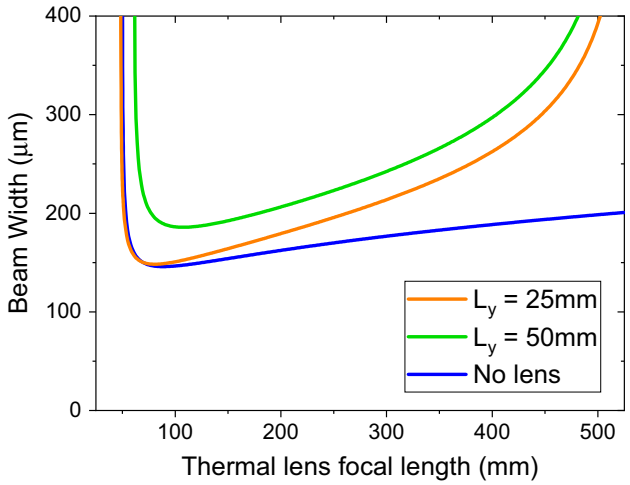

Fig. 14 Theoretical laser beam width radius at crystal as a function of thermal lens focal length for ring laser

formula at a reference plane after a single round trip with two thermal lenses f at either side of the crystal. Figure 14 shows the laser beam width radius at the crystal (left-hand side) as a function of the thermal lens focal length with $f_{-} = -250$ mm and $L_x = 25$ mm. Cavity stability is reached at $f < 500$ mm when the combined thermal lens is strong enough to overcome the defocusing of the intra-cavity negative lens. Similar to that shown with the convex-plane cavity, the laser mode size increases with cavity length but the stability range shortens.

$L_y = 25$ mm and $L_y = 50$ mm were tested with an optimum result of 4 W of total laser power (sum of bidirectional outputs) at 27.1 W of absorbed pump power with a near-diffraction limited beam quality of $M^2 < 1.1$. Both systems had a high threshold of 15 W and displayed a power roll-over at the 3-4 W level due to the cavity approaching instability, as shown in Fig. 15.

Figure 14 also shows the beam width for the ring cavity with $L_x = L_y = 25$ mm without any intra-cavity lens. The benefit of this setup is that the initial dioptric power of the thermal lens is significantly lower due to the lower

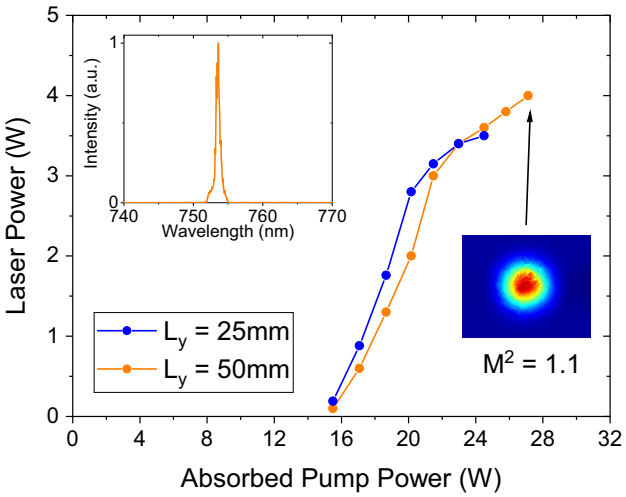

Fig. 15 Power curve for ring cavity with $f = -250$ mm lens

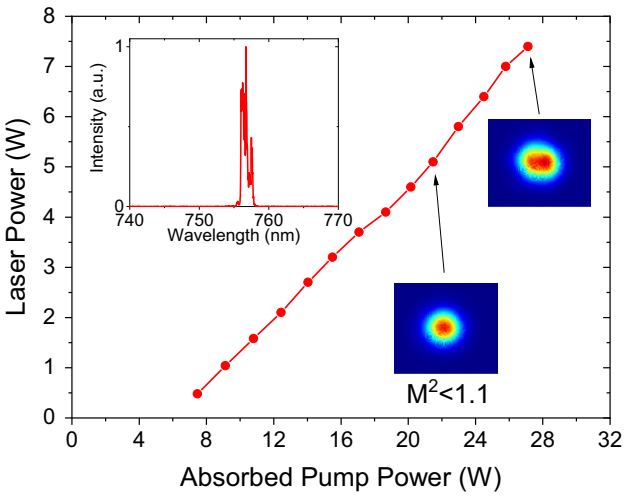

Fig. 16 Power curve for lens-free ring cavity

threshold. The cavity length is simply adjusted to provide the best matching to the pump size. For SLM operation, an intra-cavity unidirectional device would also need to be included. Due to the relatively low emission cross-section of Alexandrite, losses from intra-cavity components have a significant effect on the overall efficiency (AR coatings need to be ideally < 0.2%). Therefore, it is of additional advantage to minimise the number of components such as lenses in addition to the unidirectional device. Furthermore, removal of the internal lens provides a lower laser threshold and, therefore, a weaker population lens at the onset of lasing. This should lessen the likelihood of roll-over at the 3-4 W level.

Figure 16 shows the laser power as a function of the absorbed pump power for the ring cavity without any intra-cavity lens. 7.5 W was obtained at 27.1 W of absorbed pump

power corresponding to an optical efficiency of 28% and a slope efficiency of 35% with no indication of roll-over. The beam quality at the maximum power was $M_x^2 = 1.85$, $M_y^2 = 1.60$. Better beam quality was obtained at lower power with $M^2 < 1.1$ measured at a laser power of 5.1 W. To the best of our knowledge, these power levels are the highest obtained for an Alexandrite ring laser and show potential for a multi-watt SLM Alexandrite laser which is currently in progress.

4 Conclusion

In this work, we have presented several cavity designs for achieving multi-watt levels of output power from a diode-pumped Alexandrite in near-diffraction limited mode ($M^2 < 1.1$). This paper has shown that using the thermal lens together with convex mirror, high brightness and high power can be achieved with a maximum output power of 8.6 W with $M^2 < 1.1$ demonstrated. A detailed description of the cavity setup and modelling has also been provided and we believe it could be of use to other researchers examining power scaling of rod-type gain media. 7.5 W with 27% optical efficiency was also demonstrated using a four-mirror ring laser.

We believe that a plane-mirror ring laser to be the most suitable for diode-pumped Alexandrite SLM lasers owing to the low-loss requirements. The main challenge for this work will be obtaining low-loss (< 0.1%) intra-cavity isolator devices and packaging of all optical components into a small footprint.

Altogether, these results demonstrate the power capabilities of diode-pumped Alexandrite lasers across the 720–820 nm range—superior to any other diode-pumped vibronic laser. Its low cost, compactness and ruggedness make it an ideal laser source for growing applications in the near-infrared and ultraviolet ranges.

Author Contributions GT wrote the main manuscript and prepared all figures and data. GT and AM obtained experimental data. All authors contributed to the conception and reviewed the manuscript.

Funding This study was funded by an EPSRC Impact Acceleration Account Knowledge Transfer Secondment EP/R511547/1.

Data availability The data generated and analysed during the current study are available from the corresponding author on reasonable request.

Declarations

Conflict of interest The authors have no relevant financial or non-financial interests to disclose. The authors declare no competing interests.

References

1. J. Walling, O. Peterson, H. Jenssen, R. Morris, E. O'Dell, Tunable alexandrite lasers. IEEE J. Quant. Electron. **16**(12), 1302–1315 (1980). https://doi.org/10.1109/JQE.1980.1070430
2. G. Tawy, A. Minassian, M.J. Damzen, High-power 7.4W TEM00 and wavelength tunable alexandrite laser with a novel cavity design and fibre-coupled diodepumping. OSA Contin. **3**(6), 1638–1649 (2020). https://doi.org/10.1364/OSAC.393914
3. A.T. Coney, M.J. Damzen, High-energy diode-pumped alexandrite amplifier development with applications in satellite-based lidar. J. Opt. Soc. Am. B **38**(1), 209–219 (2021). https://doi.org/10.1364/JOSAB.409921
4. A. Munk, M. Strotkamp, B. Jungbluth, J. Froh, T. Mense, A. Mauer, J. Höffner, Rugged diode-pumped alexandrite laser as an emitter in a compact mobile lidar system for atmospheric measurements. Appl. Opt. **60**(16), 4668–4679 (2021). https://doi.org/10.1364/AO.422634
5. C. Cihan, C. Kocabas, U. Demirbas, A. Sennaroglu, Graphene mode-locked femtosecond Alexandrite laser. Opt. Lett. **43**(16), 3969–3972 (2018). https://doi.org/10.1364/OL.43.003969
6. P.F. Moulton, J.G. Cederberg, K.T. Stevens, G. Foundos, M. Koselja, J. Preclikova, Optimized InGaN-diode pumping of Ti:sapphire crystals. Opt. Mater. Express **9**(5), 2131–2146 (2019). https://doi.org/10.1364/OME.9.002131
7. A. Dergachev, J.H. Flint, Y. Isyanova, B. Pati, E.V. Slobodtchikov, K.F. Wall, P.F. Moulton, Review of multipass slab laser systems. IEEE J. Sel. Top. Quant. Electron. **13**(3), 647–660 (2007). https://doi.org/10.1109/JSTQE.2007.897177
8. U. Demirbas, I. Baali, Power and efficiency scaling of diode pumped cr: lisaf lasers: 770–1110 nm tuning range and frequency doubling to 387–463 nm. Opt. Lett. **40**(20), 4615–4618 (2015). https://doi.org/10.1364/OL.40.004615
9. U. Demirbas, I. Baali, D.A.E. Acar, A. Leitenstorfer, Diode-pumped continuous-wave and femtosecond cr:licaf lasers with high average power in the near infrared, visible and near ultraviolet. Opt. Express **23**(7), 8901–8909 (2015). https://doi.org/10.1364/OE.23.008901
10. T. Takano, H. Ogawa, C. Ohae, M. Katsuragawa, 10 w injection-locked single-frequency continuous-wave titanium:sapphire laser. Opt. Express **29**(5), 6927–6934 (2021). https://doi.org/10.1364/OE.415583
11. E. Kifle, P. Loiko, C. Romero, J.R. Vázquez de Aldana, M. Aguiló, F. Díaz, P. Camy, U. Griebner, V. Petrov, X. Mateos, Watt-level ultrafast laser inscribed thulium waveguide lasers. Progress Quant. Electron. **72**, 100266 (2020). https://doi.org/10.1016/j.pquantelec.2020.100266
12. Z. Pan, L. Wang, J.E. Bae, F. Rotermund, Y. Wang, Y. Zhao, P. Loiko, X. Mateos, U. Griebner, V. Petrov, W. Chen, Swcnt-sa mode-locked tm, ho:lclngg laser. Opt. Express **29**(24), 40323–40332 (2021). https://doi.org/10.1364/OE.445584
13. G. Tawy, J. Wang, M.J. Damzen, Pump-induced lensing effects in diode pumped Alexandrite lasers. Opt. Express **27**(24), 35865–35883 (2019). https://doi.org/10.1364/OE.27.035865
14. G. Tawy, J. Wang, M.J. Damzen : Thermal and population induced lensing in Alexandrite lasers. In: Kudryashov, A.V.,

Paxton, A.H., Ilchenko, V.S., Armani, A.M. (eds.) Laser Resonators, Microresonators, and Beam Control XXII, vol. 11266, p. 1126616. SPIE (2020). https://doi.org/10.1117/12.2542289. International Society for Optics and Photonics

15. A. Teppitaksak, A. Minassian, G.M. Thomas, M.J. Damzen, High efficiency >26 W diode end-pumped Alexandrite laser. Opt. Express **22**(13), 16386–16392 (2014). https://doi.org/10.1364/OE.22.016386
16. X. Sheng, G. Tawy, J. Sathian, A. Minassian, M.J. Damzen, Unidirectional single-frequency operation of a continuous-wave Alexandrite ring laser with wavelength tunability. Opt. Express **26**(24), 31129–31136 (2018). https://doi.org/10.1364/OE.26.031129
17. J. Sathian, G. Tawy, X. Sheng, A. Minassian, M.J. Damzen, Nonastigmatic alexandrite ring laser design with wavelength-tunable single-longitudinal-mode operation. J. Opt. Soc. Am. B **37**(7), 2185–2192 (2020). https://doi.org/10.1364/JOSAB.395394